Derivation of Mathematical Model Based on Tafel Equation Explains Microbial Fuel Cell Performance

G. Hernández-Flores[1], H. M. Poggi-Varaldo[1,*], O. Solorza-Feria[2], M. T. Ponce Noyola[3], T. Romero-Castañon[4] and N. Rinderknecht-Seijas[5]

[1]Environmental Biotechnology and Renewable Energies R&D Group, Dept. of Biotechnology and Bioengineering, Centro de Investigación y de Estudios Avanzados del Instituto Politécnico Nacional. Av. Instituto Politécnico Nacional 2508, Col. San Pedro Zacatenco, Delegación Gustavo A. Madero, México D.F., C. P. 07360 Apartado Postal: 14-740, 07000 México, D.F.
[2]Dept. of Chemistry, *ibídem.* Av. Instituto Politécnico Nacional 2508, Col. San Pedro Zacatenco, Delegación Gustavo A. Madero, México D.F., C. P. 07360 Apartado Postal: 14-740, 07000 México, D.F.
[3]Dept. Biotechnology and Bioengineering, *ibídem.* Av. Instituto Politécnico Nacional 2508, Col. San Pedro Zacatenco, Delegación Gustavo A. Madero, México D.F., C. P. 07360 Apartado Postal: 14-740, 07000 México, D.F.
[4]Electric Research Institute. Reforma 113, Col. Palmira, C. P. 62490 Cuernavaca, Morelos, México.
[5]ESIQIE del IPN, Division of Basic Sciences. Escuela Superior de Ingeniería Química e Industrias Extractivas, ESIQIE. Edificio N° 7, Unidad Profesional Adolfo López Mateos. Colonia Lindavista, Delegación Gustavo A. Madero, México D.F., C. P. 07738.
*Author for correspondence: Tel: +52 (55) 5747 3800 ext 4321 & 4324; r4cepe@yahoo.com

ABSTRACT

The aim of this work was to establish a mathematical model based on Tafel equation to quantitatively relate the maximum volumetric power ($P_{V,max}$) as well as the internal resistance (R_{int}) in a Microbial Fuel Cell (MFC), with the specific surface area of the graphite anodes (A'_s), and either their conductance C or electrolytic conductivity σ of the material.
The *MFC* consisted of a horizontal cylinder built in Plexiglas 80 mm long and 57 mm internal diameter. The anodic chamber was packed with the different anodic materials (graphite rod (*GR*), triangles of graphite (*GT*) and graphite flakes (*GF*)).
The R_{int} were 795, 410 and 273 Ω for *GR*, *GT* and *GF*, respectively, whereas the $P_{V,max}$ were 1326, 2108 and 3052 mW/m^3 for *GR*, *GT* and *GF*, respectively. There was a correspondence of either the decrease of R_{int} or the increase of $P_{V,max}$ with the increase of the log of A'_s of the graphite anodic materials. Here we show the detailed derivation of a mathematical model for the $P_{V,max}$ and R_{int} based on Tafel equation for the cell potential; it lead to equations that exhibited a good correlation with experimental results. The best fitting models for $P_{V,max}$ were $P_{V,max} = a_0' + a_1' \times \log A'_s$ and $P_{V,max} = a_0' + a_1' \times \log A'_s + a_2' \times C$ with determination coefficients 0.8872 and 0.9842, respectively. On the other hand for R_{int} the best fitting models were $R_{int} = b_0' + b_1' \times \log A'_s$ and $R_{int} = b_0' + b_1' \times \log A'_s + b_2' \times \log C$, with determination coefficients 0.8850 and 0.8904, respectively. In general, the inclusion of the electrolytic conductivity did not improve model fitting, whereas the inclusion of conductance lead to a higher determination coefficient in the P_V model but not in the model of R_{int}.

Keywords: Mathematical Model; Volumetric Power; Microbial Fuel Cells

Introduction

The imminent fossil fuels depletion and their adverse effects on the environment have resurrected the interest in bioenergies as well as other renewable energy sources [1,2]. In processes such as biohydrogen production from fermentation of organic wastes, the complete conversion of wastes to energy is not possible [3]. Dark fermentation of organic substrates effects a partial degradation of the organic matter, and typically a large amount of organic metabolites remain in the spent liquors that can be used as substrate in microbial fuel cells (*MFCs*) [4-6].

In this regard, *MFCs* constitute a promising technology for sustainable production of alternative energy and treatment of wastes such as the spent liquors of dark fermentation. A microbial fuel cell (*MFC*) is an electro-biochemical reactor capable of directly converting organic matter into electricity. In the anodic chamber the microorganisms anaerobically oxidize the organic matter and release electrons and protons. The electrons are transported to the anode that acts as an intermediate, external electron acceptor. The electrons flow through an external circuit where there is a resistor or a device to be powered, producing electricity. Electrons finally react at the cathode with protons and molecular oxygen producing water [5-9].

There are some factors that affect the electric energy production in a *MFC*, such as the nature of the biocatalysts, the type and materials of electrodes, electrode catalysts, cell configuration, and architecture, among others [10-13]. The *MFC* performance is usually restricted by ohmic overpotential, also known as internal resistance (R_{int}).

This translates into a loss of voltage that is required to drive the electron and proton transport processes. The ohmic losses in an *MFC* include both the resistance to the flow of electrons through the electrodes and interconnections and the resistance to the flow of ions through the membrane and the anodic and cathodic electrolytes (only anodic electrolyte in a single chamber *MFC*) [14]. This results in ohmic losses whose reduction or mitigation is crucial for improving the characteristics and performance of the *MFC* [15]. Furthermore, another significant role of R_{int} is related to the eventual operation of the *MFC*, since Jacobi's Theorem demonstrated that the maximum power output of an electromotive force is achieved when it is connected to an external resistance equal to its R_{int} [14-20].

The R_{int} of a *MFC* depends on some factors such as the surface area of electrodes, distance between electrodes, anodic material conductivity, the presence or absence membrane, the type of electrolyte(s), *inter alia* [14,21,22].

Indeed, the anodic material plays an important role on R_{int}. A good anodic material should have the following properties: high electrical conductivity, strong biocompatibility, chemical stability and anti-corrosion, large surface area and appropriate mechanical strength and toughness [13,14].

In order to reduce the R_{int} of the cell some materials and designs have been evaluated, such as new anodic materials, replacement of the salt bridge by membranes, choosing membranes with high protonic conductivity or building membrane-less *MFC*, increasing solution conductivity and reducing the pH, reducing electrode spacing, among others [5,6,23-29].

Regarding the effect of anodic materials, there has been much research on the use of graphite anodes in *MFC* [11-14, 28-35, among others]. However, less has been published on the effect of the specific surface area of graphite anodes on *MFC* characteristics and performance in terms of the volumetric power. On the other hand, to the best of our knowledge there is little information on modelling the effect of the anodic specific surface area on performance of *MFC* [36-38].

For instance, Hsu *et al.* [36] fitted the current intensity *i* to the anode surface area. This model gave an inverse relationship between the variables.

$$i = \frac{(mE_{anode}+b)}{A_{anode}} \qquad R^2 \text{ not reported} \qquad (1)$$

where *i* is the current density, E_{anode} is the anodic potential, A_{anode} is the surface area of the anode, m and b are fitting coefficients.

Incidentally, Hsu *et al.* [36] experimentally observed, but did not model, the decrease of the surface power densities P_{An} when the anode surface area was increased. They reported the values of P_{An} but they neither modelled

the effect of the anodic surface area (or the specific surface area) on that variable nor the volumetric power of the cell. To some extent, the decrease of P_{An} with increase of anode area should be expected whenever the increase of P_{MFC} is less than proportional to such an area. Furthermore, the model of Hsu *et al.* [36] was strictly empirical since it was not based upon electrochemical theoretical considerations. The authors did not report statistical parameters of the model, and consequently, it is very difficult to ascertain the goodness-of-fit of the proposed equation.

Dewan *et al.* [37] worked with several anodic areas (graphite plates) in a two-chamber *MFC*. They modelled the P_{An} versus the logarithm of the total surface area of the anode. They found a linear, decreasing relationship (Eq. 2, R^2 = 0.95). It can be seen that the coefficient of the term ln (surface area) is negative, which was consistent with the experimental results of Hsu *et al.* [36]. As we commented above, it is debatable to use P_{An} as a variable for comparison of process intensity. In this regard, volumetric power P_V is the dependent variable of choice. On the other hand, P_{An} is an adequate variable to assess anode performance. The model fitted by Dewan *et al.* [37] was strictly empirical since it was not based upon electrochemical theoretical considerations. No statistical parameters of goodness-of-fit were reported, other than R^2.

$$P_{An} = 0.3371 - 0.0369 \times \ln(surface\ area) \qquad R^2=0.95 \qquad (2)$$

Di Lorenzo *et al.* [38] presented a "Current distribution model" that found a relationship between a variable ν (the so-called 'utilization of the electrode area', (Siemens $^{0.5}$/sec) with a set of independent variables of electrode geometry ('*L*', thickness of the anode; '*a*', specific area of the anode), the slope of the polarization curve '*s*', and the conductivity of the influent κ

$$v = L \times \left(\frac{a \times s}{k}\right)^{0.5} \qquad (3)$$

They departed from theoretical grounds (Butler-Volmer kinetics in the anode) and several simplifying assumptions.

They also defined a new variable efficiency η related to ν by Eq. 4

$$\eta = \frac{\tanh(\nu)}{\nu} \qquad (4)$$

$$\eta = \frac{\text{observed current density}}{\text{current obtained if the electrode potential was equal to the maximum observed at position L in the electrode}} \qquad (5)$$

As a working example of their model, the authors calculated the current density peak i_2 during batch operation of a *MFC* based on a known current density peak i_1, the corresponding values of L (L_1 and L_2), and the corresponding values of η, with an equation (not given by the authors and recreated by us).

$$i_2 = i_1 \times \left(\frac{L_2}{L_1}\right) \times \left(\frac{\eta_2}{\eta_1}\right) \qquad (6)$$

They showed that their model could give reasonable results compared to experimental values of current density peaks in a couple of their experimental cases. However, in their work

(*i*) they did not develop any general fitting of Eq. 3 to 5. Furthermore, they did not report any statistical measure of good fitness (no determination coefficients, no ANOVA of the model equations and predictions, etc.);

(*ii*) they did not fit any model with volumetric power or internal resistance as dependent variable and the specific surface area of the anode as independent variable, *i.e.*, their model was used just to approximately predict current density peaks but not powers (neither P_V nor P_{An}).

(*iii*) the physical meaning of the variable ν given by the authors is vague. Furthermore, in spite of considerable work load to develop an expression for ν, this variable is only used as a 'transition' one in order to calculate the corresponding value of η.

In the end, Di Lorenzo *et al.* [38] concluded that, in spite of several recognized simplifying assumptions, the model could be useful as a starting point in selecting electrode geometries based on basic data of the influent and electrode conductivity.

Interestingly, the use of either *i* or P_{An} in the above mentioned models is very debatable as a means to express the *MFC* performance when the purpose is to compare the process intensity (unit power delivery) of a given *MFC* to the intensity of other competing processes such as other *MFC* configurations, anaerobic digestion, biohydrogen generation, etc., that could use the same influent as the main experiment. Indeed, the volumetric power is the variable to consider for a fair comparison of different processes (39,40).

Thus, the objective of this work was to establish a mathematical model based on Tafel equation to quantitatively relate the maximum volumetric power ($P_{V,max}$) as well as the R_{int} in a *MFC*, with the specific surface area (A'_s) of the graphite anodes and either their conductance *C* or electrolytic conductivity σ of the material.

Experimental

Model development

We describe a full version of the derivation of our model. A typical form of Tafel equation that relates the overpotential with the current density is given by Castellan [41].

$$\Delta V = a + b \times \ln(i) \tag{7}$$

where ΔV is the overpotential, V; *b* is the "Tafel slope", V; *i* is the current density, A/m^2.
It can be shown that

$$a = -b \times \ln(i_0) \tag{8}$$

where i_0 is the "exchange current density", A/m^2
Substituting Eq. 8 into Eq. 7, and taking logarithms in base 10 instead of base e, leads to

$$\Delta V = k \log\left(\frac{i}{i_0}\right) \tag{9}$$

where

$$k = b \times 2.303 \tag{10}$$

The actual potential delivered by the *MFC* can be expressed as the reversible potential minus the overvoltage, as in Eq. 11 (15,20)

$$E = E_{rev} - \Delta V = E_{rev} - k \log\left(\frac{i}{i_0}\right) \tag{11}$$

where *E* is the actual cell voltage; E_{rev} is the reversible potential (thermodynamic potential [41]), in V; ΔV is the overpotential, in V.

Substituting Eq. 9 into Eq. 11 we obtain the following

$$E = E_{rev} - k\ \log\left(\frac{i}{i_0}\right) \tag{12}$$

In turn, the power *P* delivered by the cell is given by [5]:

$$P = \frac{E^2}{R_{ext}} \tag{13}$$

where R_{ext} is the external resistance connected to the cell circuit, in Ω
Substituting Eq. 12 into 13 we obtain the following

$$P = \frac{\left(E_{rev} - k\ \log\left(\frac{i}{i_0}\right)\right)^2}{R_{ext}} \tag{14}$$

Doing the algebra, taking into account that $\Delta V < E_{rev}$, and that $i = I/A_{el}$, plus some simplifications based on order of magnitude of selected terms, leads to

$$P = \frac{E_{rev}^2 - 2klog\left(\frac{i}{i_0}\right) + k^2\left(log\frac{i}{i_0}\right)^2}{R_{ext}} \tag{15}$$

$$P = \frac{E_{rev}^2 - 2k(\log i - \log i_0) + k^2[(\log i)^2 - 2\log i * log\ i_0 + (\log i_0)^2]}{R_{ext}} \tag{16}$$

Since $\Delta V < E_{rev}$, we can neglect the term $(log\ i_0)^2$ in Eq. 16, leading to

$$P \cong \frac{E_{rev}^2 + 2klogi_0 - 2klogi}{R_{ext}} \tag{17}$$

By definition, the current intensity can be expressed as [17,41]

$$i = \frac{I}{A_{el}} \tag{18}$$

where
I is the current intensity in Amperes
A_{el} is the electrode surface area in m^2

Substituting Eq. 18 into Eq. 17 leads to

$$P \cong \frac{E_{rev}^2 + 2klogi_0 - 2klog\left(\frac{I}{A_{el}}\right)}{R_{ext}} \tag{19}$$

and

$$P \cong \frac{E_{rev}^2 + 2klogi_0 - 2klogI + 2klogA_{el}}{R_{ext}} \tag{20}$$

$$P \cong \frac{(E_{rev}^2 + 2klogi_0 - 2klogI) + 2klogA_{el}}{R_{ext}} \quad (21)$$

We recall that the specific area of the electrode A'_s can be determined dividing the electrode surface area A_{el} by the cell volume V_{cell} (the anodic chamber volume in unicameral *MFC*),

$$A'_s = \frac{A_{el}}{V_{cell}} \quad (22)$$

$$A_{el} = V_{cell} A'_s \quad (23)$$

On the other hand, the volumetric power P_V of a *MFC* is given by the Eq. 24 below [28]

$$P_V = \frac{P}{V_{cell}} \quad (24)$$

Substituting Eq. 21 in the Eq. 24

$$P_V \cong \frac{(E_{rev}^2 + 2klogi_0 - 2klogI)}{R_{ext}V_{cell}} + \left(\frac{2k}{R_{ext}V_{cell}}\right) \log A_{el} \quad (25)$$

Now, we substitute Eq. 23 in Eq. 25

$$P_V \cong \frac{(E_{rev}^2 + 2klogi_0 - 2klogI)}{R_{ext}V_{cell}} + \left(\frac{2k}{R_{ext}V_{cell}}\right) \log(V_{cell}A'_s) \quad (26)$$

Regrouping terms leads to

$$P_V \cong \frac{(E_{rev}^2 + 2klogi_0 - 2klogI)}{R_{ext}V_{cell}} + \frac{2klogV_{cell}}{R_{ext}V_{cell}} + \frac{2k}{R_{ext}V_{cell}} \log A'_s \quad (27)$$

$$P_V \cong \frac{(E_{rev}^2 + 2klogi_0 - 2klogI + 2klogV_{cell})}{R_{ext}V_{cell}} + \frac{2k}{R_{ext}V_{cell}} \log A'_s \quad (28)$$

The first term of the left hand member of Eq. 28 is nearly a constant and it will denoted as a_o, whereas the parameters in the logarithmic term will be denoted as the coefficient a_1

$$a_0 = \frac{(E_{rev}^2 + 2klogi_0 - 2klogI + 2klogV_{cell})}{R_{ext}V_{cell}} \quad (29)$$

$$a_1 = \frac{2k}{R_{ext}V_{cell}} \quad (30)$$

So,

$$P_{V,max} \cong a_0 + a_1 \log A'_s \quad (31)$$

Now, to estimate the R_{int}, we know that maximum volumetric power $P_{v,max}$ occurs when the external resistance R_{ext} connected to the circuit of an electromotive force is equal to the value of the internal resistance R_{int}. This is a result of Jacobi's theorem of electromotive forces [17,20,28].

$$R_{int} = R_{ext} \quad (32)$$

By definition of power *P* in direct current circuits and Jacobi's theorem, then

$$P = \frac{(E_{MFC,max})^2}{R_{int}} \quad (33)$$

where

$E_{MFC,max}$ is the cell potential at which the maximum volumetric power is registered. Introducing the volume V_{cell} for converting the power into volumetric power, and solving Eq. 33 for R_{int} leads to

$$R_{int} = \frac{(E_{MFC,max})^2}{V_{cell} P_{V,max} F} \quad (34)$$

V_{cell} is the cell volume or the anodic chamber volume in a unicameral *MFC*

$P_{V,max}$ maximum volumetric power

F is a unit conversion factor that, for example, takes into account that the volumetric power is usually expressed in mW/m^3, etc.

Substituting Eq. 31 into Eq. 34 and rearranging

$$R_{int} = \frac{(E_{MFC,max})^2}{V_{cell} F} \frac{1}{a_0 + a_1 \log A's} \quad (35)$$

$$R_{int} = \frac{(E_{MFC,max})^2}{V_{cell} F a_0 \left(1 + \frac{a_1}{a_0} \log A's\right)} \quad (36)$$

When a given amount β is $\beta < 1$, the following approximation can be used [42]

$$\frac{1}{1+\beta} \cong 1 - \beta \quad (37)$$

This approximation, although simple, is very good. Indeed, it can be shown that when
$\beta \leq 0.30$, the error of this formula does not exceed 10%, and when
$\beta \leq 0.10$, the error of this formula does not exceed 1% [42]
Using Eq. 37 in Eq. 36 leads to the following approximate result

$$R_{int} \cong \frac{(E_{MFC,max})^2}{V_{cell} F a_0} \left(1 - \frac{a_1}{a_0}\right) \log A'_s \quad (38)$$

Rearranging Eq. 38

$$R_{int} \cong \left(\frac{(E_{MFC,max})^2}{V_{cell} F a_0}\right) - \frac{(E_{MFC,max})^2 a_1}{V F a_0^2} \log A'_s \quad (39)$$

Now, we conveniently rename the constant coefficients of Eq. 39 as follows

$$b_0 = \frac{(E_{MFC,max})^2}{V_{cell} F a_0} \quad (40)$$

$$b_1 = -\frac{(E_{MFC,max})^2 a_1}{V_{cell} F a_0^2} \quad (41)$$

Finally, the equation for R_{int} is in the form

$$R_{int} \cong b_0 + b_1 \log A'_s \quad (42)$$

Experimental design

The first experiment consisted of the characterization of the *MFC* fitted with following anodic materials: graphite rod (*GR*), triangles of graphite (*GT*) and graphite flakes (*GF*) in an *MFC* loaded with a sulfate-reducing inoculum (*SR-In*), with two replicates. The main response variables were the $P_{V,max}$ and the R_{int} of the *MFC*s. The experiments were carried out in a single compartment, air-cathode *MFC*. The cells were operated at ambient temperature.

2.3. Microbial fuel cell

The *MFC* consisted of a horizontal cylinder built in Plexiglas 80 mm long and 57 mm internal diameter. The anodic chamber was packed with the different anodic materials, i.e., *GR*, *GT* and *GF* with corresponding surface areas of 8.89×10^{-4}, 0.06 and 0.28 m^2 (Table 1).

The *GR* was purchased to Lumen S.A. de C.V., Mexico City, Mexico; they report that this material was imported from the Czech Republic. The *GT*s were fabricated by conveniently slicing graphite bars of 38 mm diameter in disks of 5 mm thickness. Each disk, in turn, was cut in 8 similar parts. The graphite bar was purchased to Brunssen de Occidente S.A. de C.V., Guadalajara, Jalisco, Mexico.

For *GF*, we screened a large sample of material and collected the fraction between meshes 10 and 6 (diameters 2 mm and 3.55 mm, respectively). We took and weighed five 20 g subsamples of this fraction; the mass values were annotated. Afterwards, the number of particles in each subsample were determined and annotated. An average number of particles was estimated. With this number, we estimated the average weight of particle of each material. By using the equations shown below, it was possible to calculate the surface area of the mass of material loaded into the *MFC*. The shape factor of the material (also called sphericity factor in other textbooks) was taken into account as described in Perry [43]. For instance, we chose 0.43 for *GF* flakes, and 0.73 for *GAC*.

On the other hand, the net volume of the only chamber in our *MFC*s was calculated as the geometric volume of the chamber minus the physical volume of the anodic material. With the surface area of the anodic material and the net volume, the specific surface area of the anode A'_s was finally calculated with Eq. 43 below

$$A'_s = \frac{\frac{M}{\Phi_s}\left(\frac{6^2 m_p{}^2 \pi^3}{m_p{}^3 \pi^2 \rho^2}\right)^{1/3}}{V} = \frac{\frac{M}{\Phi_s}\left(\frac{36\pi}{m_p \rho^2}\right)^{1/3}}{\left(V_{cell} - \frac{M}{\rho}\right)} \quad (43)$$

where

$\bar{D}_p$ average particle diameter, defined as the diameter of a sphere of the same volume as the particle

Φ_s shape factor of the particle defined as the quotient of the area of a sphere equivalent to the volume of the particle divided by the actual surface of the particle

m_p average weight of a particle of the given size fraction

M total mass of anodic material loaded into the *MFC*
ρ actual density of the material
V_{cell} geometric volume of the cell chamber

The surface area of the graphite rod was calculated by geometric calculations based on diameter and height of the rod. The net volume of the *MFC* necessary for the denominator in the calculation of $A_s^{'}$ was estimated as described above in the denominator of Eq. 43.

Similarly, the surface area of graphite triangles was estimated by geometric calculations. For each triangular piece to be loaded into the *MFC*, the total area was the sum of the areas of the two triangular faces ((base times height/2) ×2) plus the areas of the rims. The overall surface area was estimated as the sum of the areas of the pieces. The specific surface area was finally calculated by dividing by the net volume of the *MFC*.

The cathode of our *MFC* was a flexible carbon-cloth containing 0.5 mg/cm^2 platinum catalyst (Pt 10 wt%/C-ETEK). On the air side, the cathode was limited by a perforated plate of stainless steel 1 mm thickness. In the liquid side, the cathode was in contact with a proton exchange membrane (Nafion® 117) [6,44].

2.4. Sulfate-reducing inoculum SR-In

The *MFC*s were seeded with a *SR-In* sampled from a sulphate-reducing complete mix reactor. The biomass concentration in the inoculum was *ca*. 1280 mg VSS/L. The complete mix bioreactor was operated at 37 °C in a constant temperature room. An influent containing sucrose as carbon source was fed at a flow rate of 120 mL/d to the complete mix sulphate-reducing bioreactor. Its composition was (in g/L): sucrose (5.0), acetic acid (1.5), $NaHCO_3$ (3.0), K_2HPO_4 (0.6), Na_2CO_3 (3.0), NH_4Cl (0.6), Na_2SO_4 (11.0).

2.5. Leachate

The *MFC* was loaded with 6 mL of a leachate similar to that produced in the hydrogen fermentation of the organic fraction of the municipal solid wastes [45]. The model leachate was concocted with a mixture of simple organic acids and solvents (in g/L): acetic, propionic and butyric acids (4 each) as well as acetone and ethanol (4 each) and mineral salts like $NaHCO_3$ and Na_2CO_3 (3 each) and K_2HPO_4 and NH_4Cl (0.6 each) [46,47].

2.6. Determination of internal resistance of the cell

The internal resistance of the cell was determined by duplicate for each anodic material, using the polarization curve method by varying the external resistance and recording both the voltage and the current intensity [6,28].

The *MFC* was operated at open circuit for 1 h; afterwards the R_{ext} was varied from 10 Ω to 1 MΩ and viceversa. After this, the cell was set to open circuit conditions for 1 h in order to check the adequacy of the procedure (values of initial and final open circuit voltages should be close). The voltage was measured and recorded with a Multimeter ESCORT 3146A. The current was calculated by the Ohm's law and the R_{int} was calculated as the slope of the linear section of the curve voltage versus the current intensity [6,14].

The volumetric power (P_V) was calculated according the following equation:

$$P_V = \frac{(E_{MFC})^2}{V_{cell} \times R_{ext}} \qquad (44)$$

where V_{cell} is the net volume of the cell; E_{MFC} is the voltage delivered by the cell; R_{ext} is the external resistance connected to the cell.

The initial chemical oxygen demand (COD) and biomass concentration in the cell liquor were *ca.* 1300 mg O_2/L and 1280 VSS/L respectively. The pH and the electrical conductivity were 7.03 and 1385 µS/cm respectively.

2.7. Analyses

The COD and VSS of the liquors of sulphate-reducing seed bioreactor and cells were determined according to the Standard Methods [48]. In addition, the individual concentrations of volatile organic acids and solvents in the model extract were analyzed by gas chromatography in a chromatograph Perkin Elmer Autosystem equipped with a flame ionization detector as described elsewhere [6].

Statistical data processing was performed with the tool Analysis of Data/Regression of Excel software, Microsoft Office 2010 (Microsoft, Seattle, WA, USA). Excel outputs were checked with Minitab 17 (Minitab Inc., State College, PA, USA) outputs as a quality control; the softwares gave identical results.

Results and discussion

Characterization of the cell using the anodic materials and sulphate-reducing inoculums

Table 1 exhibits some properties of the anodic materials whereas Figure 1a shows the characterization of the *MFC* fitted with *GR* as anode. The maximum OCP was 800 mV in the first hour of the characterization; at the end of the procedure the OCP was 600 mV. The R_{int} was obtained from the slope of graph voltage *vs.* current intensity and gave a value of 795 Ω (Table 2). With *GT* as anode, the estimated R_{int} was 410 Ω and the $P_{V,max}$ reached 2108 mW/m^3 (Figure 1b, Table 2), 50% lower than the R_{int} obtained by the *GR*.

Table 1. Selected physical characteristics of anodic materials

Anodic material	Working net volume (m^3)	Anodic actual surface (m^2)	*A's*[a] (m^2/m^3)	Conductance (S)[b]
Graphite rod	2.03×10^{-4}	$8.89\times10^{-4} \pm 2.5\times10^{-5}$	7.3	0.20 ± 0.04
Triangles of graphite	6.64×10^{-5}	0.062 ± 0.001	931	0.61 ± 0.02
Graphite flakes	7.22×10^{-5}	0.28 ± 0.08	1302	0.13 ± 0.04

[a] Relationship between the anode surface area to cell volume, also known as specific surface area of the anode.
[b] Electrical conductance of the materials, expressed in Siemens.

The P_V improved by 60% using the *GT* (Table 2). It is interesting to note that the ratio between specific surface areas of the corresponding anodes (anodic surface/cell volume) increased by 12700% from *GR* to *GT* (a ratio 931/7.3; Table 1). This could partially explain the lower R_{int}, although neither the power increase or the R_{int} decrease was in the same proportion ratio as the anodic surface area increase.

Regarding the *GF* used as anode, the R_{int} and $P_{V,max}$, decreased and increased respectively with respect to *GT* as anode (Fig. 2, Table 2). The R_{int} was 35% lower than *GT* and the $P_{V,max}$ reached 3052 mW/m^3, 45% more than *GT*. It is important to note that in this anode, the relationship anodic surface/cell volume increased 4 times from *GT* to *GF* (Table 1).

The larger surface area of *GF* compared to the other anodic materials would be an advantage since the microorganisms would have a greater anodic surface to colonize and transfer the electrons. In this regard, our results and interpretation are consistent with findings of other researchers [31-35].

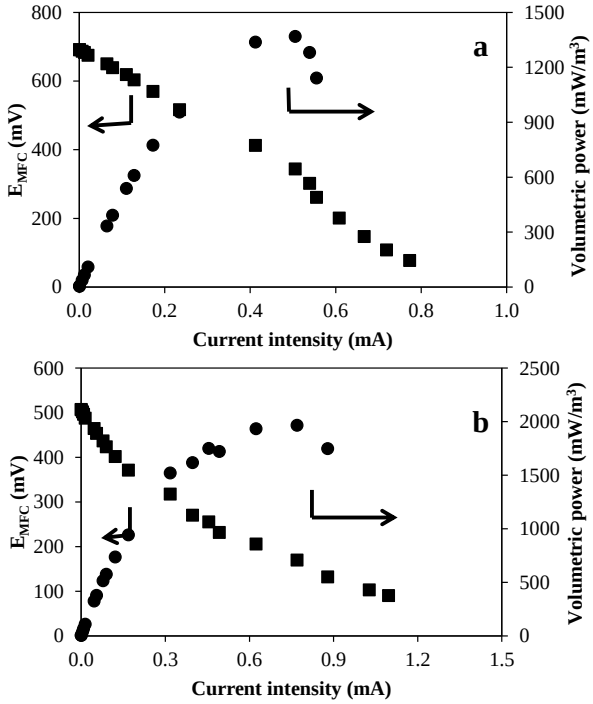

Fig 1. Characterization of the microbial fuel cell fitted either with graphite rod and graphite triangles as anode: (a) Polarization curve and volumetric power for graphite rod as anode; (b) Polarization curve and volumetric power with graphite triangles as anode.

Hays *et al.* [31] found that *MFC* equipped with graphite fiber brush electrodes and modified designs (separators with graphite brush electrodes, to make a more compact design) gave satisfactory power and potential outputs. They ascribed this to high surface areas for exoelectrogenic bacteria growth in graphite-brush-equipped *MFC*s. Feng *et al.* [32] studied the treatment of carbon fiber brush anodes for improving the power output in an air-cathode *MFC*s. They concluded first that carbon brush electrodes provided high surface areas for bacterial growth and high power densities in microbial fuel cells (*MFC*s). Second, they showed that a combined heat and acid treatment of the brush anodes lead to improved power output of the cell, 34% higher than that of the untreated control.

Larrosa-Guerrero *et al.* [33] examined the effect of various carbon anodes (graphite, sponge, paper, cloth, felt, fiber, foam and reticulated vitreous carbon (RVC)) on *MFC* performance. Brewery wastewater diluted with domestic wastewater was the model influent. Biofilms were grown at open circuit or under an external load. The average voltage output was 600 mV at closed circuit when connected to an external resistance of 300 kΩ, and 750 mV at open circuit for all materials, except RVC. They observed a poor performance of RVC compared to the other anodic materials, i.e., power densities as low as 1.3 mW/m^2. The authors concluded that this might be related to lower surface area available and concentration polarization caused by the morphology of the material and the structure of the biofilm.

Table 2. Results of characterization of the microbial fuel cells

Parameters	Graphite rod	Triangles of graphite	Graphite flakes
Inoculum	SR-In [a]	SR-In [a]	SR-In [a]
R_{int} (Ω)	795 ± 147	410 ± 22	273 ± 153
$P_{s,max}$ (mW/m^2)[b]	65.4 ± 0.1	54 ± 0.1	86.4± 0.7
$P_{V,max}$(mW/m^3)[c]	1326 ± 72	2108 ± 174	3052 ± 23
P_{max}(mW)	0.17 ± 0.01	0.14 ± 0.01	0.22 ± 0.01
I_{max} (mA)[d]	1.53 ± 0.3	1.92 ± 0.6	3.50 ± 0.6
$E_{MFC,max}$ (mV)[e]	700 ± 1	500 ± 1	402 ± 1
$E_{MFC,OC}$ (mV)[f]	800 ± 120	600 ± 140	575 ± 33

[a] Sulphate-reducing inoculum.
[b] Maximum power density based on surface area of electrode (cathode).
[c] Maximum volumetric power.
[d] Current intensity value at the maximum power.
[e] Potential value at the maximum power.
[f] Open circuit potential.

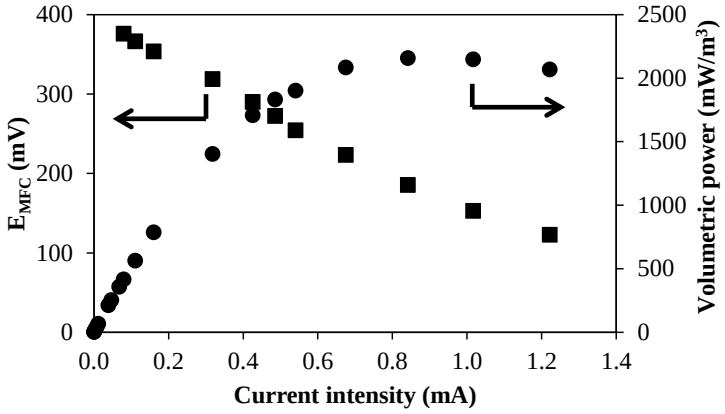

Fig 2. Polarization curve and volumetric power with graphite flakes as anode

Liu *et al.* [34] observed that the achievable maximum current density for mature microbial biofilms in *MFC* treating wastewater was strongly dependent on the electrode material, among other factors. Incidentally, the potential of the active site (-120 mV vs. SHE) was similar for all the electrocatalytically active microbial biofilms in their work, and to that observed for *Geobacter sulfurreducens* in other works. Jin *et al.* [35] tested the effect of using carbon mesh anodes modified by hydrazine hydrate chemical reduction on possible improvement of power generation in an air-cathode *MFC*.

The power densities of *MFC*s using hydrazine-treated anodes were all higher (by 31%) than that of the untreated control; coulombic efficiency increased by 24%. Such improvement in *MFC*s performance correlated with the increased surface area and the change of surface functional groups as revealed by X-ray photoelectron spectroscopy analysis. Also, the authors concluded that the anode material type and surface area are considered key factors influencing the energy conversion in *MFC*s because it links microbiology and electrochemistry. Also, the better characteristics of *MFC* fitted with graphite anodes in this work (*i.e.*, *GR*, *GT* and *GF*) compared to *GAC* could be explained by the high electric conductivity of graphite compared to the low conductivity of *GAC* (Table 1).

Modeling of the maximum volumetric power and internal resistance of microbial fuel cells equipped with graphite anodes in this work

We made an attempt to quantitatively relate the $P_{V,max}$ and R_{int} in this work to the specific surface area A'_s of the graphite anodes as well as either the conductance C or electrolytic conductivity σ of the material. We have used the six datasets for model fitting, *i.e.*, two replicates for each anodic material (2×3). A theoretical development that linked the volumetric power to the cell potential (and the latter, in turn, was expressed as the reversible potential minus the overpotential described by Tafel equation, see Section 2.1 for Model derivation) showed that $P_{V,max}$ and R_{int} could be associated to the log A'_s as follows in the Eq. 31 and 42.

$$P_{V,max} \cong a_0 + a_1 \log A'_s$$

$$R_{int} \cong b_0 + b_1 \log A'_s$$

Consequently, we postulated linear regression models of R_{int} and $P_{V,max}$ in terms of:
-the specific surface area of the electrode A'_s or its logarithm,
-the conductance C of the material of the electrode or its logarithm,
-the electrolytic conductivity σ of the material of the electrode or its logarithm
A family of uni-variable regression models (with log A'_s as the regressor variable) and bi-variable models (with log A'_s and either C or σ as or their logarithms regressor variables, without and with interaction between regressor variables) were fitted to the experimental data (Table 3). The fittings were carried out with the tool Analysis of Data/Regression of Excel 2010, Microsoft Office, Microsoft.

Table 3 shows detailed statistical information on the fitting of several models tested in our work. The selection of the recommended models was based on these criteria:

(i) Among models with similar goodness of fit, we select the one or those that has/have a theoretical basis over the ones that are only empirical.

(ii) Among models with similar or reasonable goodness of fit, we choose the one or those that are more simple (lower number of independent variables, for example) because, in addition to the attractive simplicity, the regression will have higher degrees of freedom.

(iii) We recommmend models that exhibit the lowest value of probability of the Fisher statistic *p(F)*, low values are related to higher significance of ANOVA of the regression).

(iv) Models with high values of determination coefficient are good candidates for final selection, provided that other statistical parameters of the regression are also satisfactory.

(v) Models with higher values of the parameter Ranking will be preferred, provided that other statistical parameters of the regression are also satisfactory. In this regards, we have defined a convenient parameter Ranking as follows:

$$Ranking = \left(\frac{\text{Number of significant coefficients of the regression}}{\text{Number of total coefficients}}\right) \times 100 \qquad (45)$$

In this work, a coefficient of the regression equation is defined as 'significant' (stands for 'this work') when its confidence interval 95% does not contain the zero (0), although the statistical significance of a coefficient is given by the corresponding value *p(T)*. Generally, a low value of *p(T)* indicates a statistically significant coefficient.

Based on the application of these criteria we have chosen five models that could adequately fit our experimental results. Three models for the volumetric power (Eq. 46 to 48; models 1, 3, and 5; Table 3) and two models for the internal resistance of the *MFC* (Eq. 49 and 50; models 2, 16; Table 3).

1.- $P_{V,max} \cong a_0{}' + a_1{}' \log A'_s$ (46)

3. $P_{V,max} \cong a_0 + a_1 \log A'_s + a_2 \times C$ (47)

5. $P_{V,max} \cong a_0' + a_1{}' \times \log A'_s + a_2{}' \times \log C$ (48)

2. $R_{int} \cong b_0{}' + b_1{}' \times \log A'_s$ (49)

16. $R_{int} \cong b_0 + b_1 \times \log A'_s + b_2 \times \sigma + b_{12} \times [(\log A'_s) \times \sigma]$ (50)

Table 3. Model fitting of either maximum volumetric power or internal resistance with the specific area of anodes and other variables this work

Model Regression equation	R^{2a}	a_0' or b_0' [b]	a_1' or b_1' [c]	a_2' or b_2' [d]	a_{12}' or b_{12}' [e]	Ranking[f] (%)	p(F)[g]
1. $P_{V,max}=a_0'+a_1'\times\log A'_s$	0.8872	842.9*	633.2*	NA[h]	NA[h]	100	0.005
2. $R_{int}=b_0'+b_1'\times\log A'_s$	0.8850	933.5*	-211.6*	NA[f]	NA[h]	100	0.005
3. $P_{V,max}=a_0+a_1\times\log A'_s+a_2\times C$	0.9842	1133.66*	660.73*	-1046.79*	NA[h]	100	0.002
4. $R_{int}=b_0+b_1\times\log A'_s+b_2\times C$	0.8865	922.15*	-212.75*	43.69	NA[h]	67	0.038
5. $P_{V,max}=a_0'+a_1'\times\log A'_s+a_2'\times\log C$	0.9810	403.2	629.8*	-738.69*	NA[h]	67	0.003
6. $R_{int}=b_0'+b_1'\times\log A'_s+b_2'\times\log C$	0.8904	968.9*	-211.3*	59.46	NA[h]	67	0.036
7. $P_{V,max}=a_0+a_1\times\log A'_s+a_2\times C+a_{12}\times[(\log A'_s)\times C]$	0.9861	1569.97	493.39	-3387.82	917.61	0	0.021
8. $R_{int}=b_0+b_1\times\log A'_s+b_2\times C+b_{12}\times[(\log A'_s)\times C]$	0.9124	353.21	-4.11	2962.56	-1144.1	0	0.128
9. $P_{V,max}=a_0'+a_1'\times\log A'_s+a_2'\times\log C+a_{12}'\times[(\log A'_s)\times(\log C)]$	0.9833	-402.11	949.48	-1864.23	427.92	0	0.025
10. $R_{int}=b_0'+b_1'\times\log A'_s+b_2'\times\log C+b_{12}'\times[(\log A'_s)\times(\log C)]$	0.9081	1720.77	-509.79	1110.44	-399.57	0	0.135
11. $P_{V,max}=a_0+a_1\times\log A'_s+a_2\times\sigma$	0.9277	-318.23	1026.97*	1.61	NA[h]	33	0.019
12. $R_{int}=b_0+b_1\times\log A'_s+b_2\times\sigma$	0.9052	658.72	-118.45	0.38	NA[h]	0	0.029
13. $P_{V,max}=a_0+a_1'\times\log A'_s+a_2'\times\log\sigma$	0.9732	-3583.09	1507.69*	1423.86	NA[f]	33	0.004
14. $R_{int}=b_0'+b_1'\times\log A'_s+b_2'\times\log\sigma$	0.8918	517.10	-129.35	133.94	NA[f]	0	0.036
15. $P_{V,max}=a_0+a_1\times\log A'_s+a_2\times\sigma+a_{12}\times[(\log A'_s)\times\sigma]$	0.9401	-382.66	1286.00	10.09	-13.47	0	0.089
16. $R_{int}=b_0+b_1\times\log A'_s+b_2\times\sigma+b_{12}\times[(\log A'_s)\times\sigma]$	0.9923	715.79*	-347.90*	-7.13*	11.93*	100	0.012
17. $P_{V,max}=a_0'+a_1'\times\log A'_s+a_2'\times\log\sigma+a_{12}'\times[(\log A'_s)\times(\log\sigma)]$	0.9732	-3581.61	1514.17	1425.54	-5.78	0	0.040
18. $R_{int}=b_0'+b_1'\times\log A'_s+b_2'\times\log\sigma+b_{12}'\times[(\log A'_s)\times(\log\sigma)]$	0.9595	350.38	-857.95	-54.84	649.40	0	0.060

[a] Determination coefficient; [b] independent term of the equation; [c] coefficient of the variable log A'_s; [d] coefficient of the second variable C, σ, log C or log σ; [e] coefficient of the third variable 'crossed product' of the first and second variable; [f] Ranking = (Number of significant coefficients of the regression/Number of total coefficients) *100; 'significant coefficients' are those whose confidence interval does not include zero (0); [g] probability of the Fisher statistics in the ANOVA of the regression; [h] not applicable; *the star on the right side of the coefficient values means that their values were statistically significant and that zero did not belong to their 95% confidence intervals.

Among these models, we feel that the most recommendable are the No 1 and 2 (Eq. 46 and 49) since they show an adequate set of statistical parameters and at the same time are the most simple (one independent variable) and their mathematical forms are based on a theoretical derivation (Tafel equation for overvoltage of the *MFC* plus ancillary concepts). Standardized residuals of our selected models were higher than -2 and lower than 2, which suggests the absence of wild data (outliers) [49].

As a worked example on how the selection process proceeds, let us focus the attention on model 17 for $P_{V,max}$ (Table 3). This model was not chosen to represent our data in spite that the regression shows a high R^2, because

-the model is more complex (3 independent variables, or two independent variables plus their interaction, as one prefers to consider it),

-two terms of the regression are not related to basic electrochemical mechanisms of the device (the second and the third terms of the right member), in fact, these two terms could be considered as empirical "crutches"

-the *p(F)* of the ANOVA of the regression is relatively high compared to those of other models

-the Ranking is 0%, that is, the confidence intervals of all the regression coefficients contain zero (0).

The fitting of our model to data published by Dewan *et al.* [37] was also performed. Their goal was to quantify the relationship, if any, between the surface area of the anode of a two-chamber *MFC* and the anodic power density (surface). Graphite plate electrodes of various sizes were used as anodes. The cathode consisted of Mn-based catalyzed carbon bonded to a Pt mesh that performed as current-collector device. They found that the power density (surface) P_{An} decreased as the surface area of the anode increased; the relationship was decreasingly linear when the P_{An} was plotted against log of the surface area of the anode.

Unfortunately, they neither used the *specific surface area* A'_s of the anode (just the plain surface area) nor performed any study on the relationship between the *volumetric power* P_V and A'_s.

From data in their 'Materials and Methods' section as well as their results from the 'Results and discussion' section (Fig. 2b in their article), we calculated the $P_{v,max}$ and the A'_s. Afterwards, we applied our most simple model $P_{v,max}$ versus log (A'_s) (Model 1 in Table 3, Eq. 46). We found that our model adequately fitted their experimental results (Eq. 51 below)

$$P_{V,max} \cong 0.0348 + 0.01437 \times \log A'_s \qquad (51)$$

with $P_{V,max}$ in mW/cm^3, A'_s in cm^2/cm^3

The statistical parameters were the following:

R^2 = 0.8704; *p(F)* = 0.0022; Ranking = 100%

$0.02347 \leq a_o \leq 0.04469$ at 95% confidence, *p(T)* = 0.00042

$0.00800 \leq a_1 \leq 0.02075$ at 95% confidence, *p(T)* = 0.00216

The largest standardized residual was 1.43, whereas the smallest was -1.22. Thus, all the residuals fell in the interval (-2.0, 2.0) meaning that no outliers were found [55].

At this point, it is worth comparing our model with the previous models available in the literature. They dealt with cell performance and the surface area of the anode but focused on other dependent variables that are not useful indicators of process intensity, such as current intensity [36], peaks of current intensity [38], or P_{An} [36]. This was a first shortcoming, since the use of either *i* or P_{An} is not the most adequate variable to express the *MFC* performance when the purpose is to compare the process intensity with intensity of other competing processes such as other *MFC* configurations, anaerobic digestion, biohydrogen generation, etc.

Two of the three previous models presented in the literature did not report statistical parameters that show the goodness of fit. Only one of them [37] reported the determination coefficient of the regression, but no information on *p(F)*, confidence intervals of the regression coefficients, *etc.*, was included. So, the usefulness of such models as well as their goodness-of-fit is difficult to ascertain.

Only one of the previous models out of the three has been based on electrochemical theoretical grounds [38]. The other two are strictly empirical.

In contrast, our model focuses on the relationship of the volumetric power and internal resistance versus the specific area of anode, and it is based on electrochemical theory (Tafel equation and ancillary concepts). Moreover, thorough statistical evidence of its goodness-of-fit is provided.

Another model (Eq. 52) proposed by us, completely empirical and with no theoretical support so far, was tested for fitting results from literature and our own work (Table 4).

$$\log P_{V,max} \cong a_0 + a_1 \times \log A'_s \quad (52)$$

Table 4. Summary of fitting results of a log-log model given by Eq. 52

Model Regression equation	R^{2a}	a_0 [b]	a_1 [c]	Ranking[d] (%)	p(F) [e]	Reference
$\log P_{V,max} \cong a_0 + a_1 \times \log A'_s$	0.9970	-0.905*	0.840*	100	1.7×10^{-7}	[37]
	0.9683	-0.918	1.152*	50	0.0160	[38]
	0.9430	3.024*	0.137*	100	0.0012	This work

[a] Determination coefficient; [b] independent term of the equation; [c] coefficient of the variable log A'_s; [d] Ranking = (Number of significant coefficients of the regression/Number of total coefficients) ×100; 'significant coefficients' are those whose confidence interval does not include zero (0); [e] probability of the Fisher statistics in the ANOVA of the regression; *the star on the right side of the coefficient values means that their values were statistically significant and that zero did not belong to their 95% confidence intervals.

Transforming the log-log model (Eq. 52) to its potential form, the data from Di Lorenzo *et al.* (2010) [38]

$$\log P_{V,max} = -0.918 + 1.152 \times \log A'_s \quad (53)$$

are represented by

$$P_{V,max} = 10^{-0.918} \times A'_s{}^{1.152} \quad (54)$$

or better

$$P_{V,max} = 0.1208 \times A'_s{}^{1.152} \quad (55)$$

Similarly, data from Dewan *et al.* (2008) [37] are represented by

$$P_{V,max} = 0.1244 \times A'_s{}^{0.8404} \quad (56)$$

Whereas our own experimental data fitted by this second model gives

$$P_{V,max} = 1056.82 \times A'_s{}^{0.1373} \quad (57)$$

The table 4 shows best statistical values for the fitting of the results from literature and our own work in the log-log mathematical model. However, this mathematical model lacks of a theoretical basis. Although the good fit of the model, is not enough evidence to use this model.

Summary and perspectives

The type and size of anodic material have a significant effect on the R_{int} and $P_{V,max}$ of *MFC*s in our work. Comparing the graphite anodes, the $P_{V,max}$ increased and the R_{int} decreased in three materials (*GR*, *GT* and *GF*) with the increase of the log of the specific surface area of the anode. A theoretical model for the $P_{V,max}$ and R_{int} based on the electrochemical performance of the cell lead to equations that satisfactorily fitted the experimental results. The mathematical model leads us to predict the behavior of the performance of the *MFC*s. It is very important in order to scaling of these devices.

Finally, results of this work point out to a promising approach to further tapping bioelectricity from organic wastes that previously have yielded biohydrogen.

Acknowledgements

The authors wish to thank CINVESTAV-IPN and SECITI-GDF (formerly ICYTDF), Mexico, for financial support to this research (PICCO-10-28). Giovanni Hernandez-Flores received a graduate scholarship from CONACYT, Mexico. Also the authors thank Mr. Rafael Hernández-Vera, and technicians of the Environmental of Biotechnology and Renewable Energy R&D Group, CINVESTAV-IPN for their excellent technical help.

References

[1] D. Das, T. N. Veziroglu, Hydrogen production by biological processes: a survey of literature. Int J. Hydrogen Energy 2001; 26:13-28
[2] Y. Cheng-Dar, L. Chung-Ming, E. M. L. Liou, A transition toward a sustainable energy future: feasibility assessment and development strategies of wind power in Taiwan. Energy Policy 2001; 29: 951-963
[3] I. Valdez-Vázquez, E. Ríos-Leal, F. J. Esparza-García, F. Cecchi, H. M. Poggi-Varaldo, Semi-continuous solid substrate anaerobic digestors for H_2 production from organic waste: Mesophilic versus thermophilic regime. Int. J. Hydrogen Energy 2005; 30: 1383-1391
[4] I. Valdez-Vazquez, E. Rios-Leal, A. Carmona-Martinez, K. Muñoz-Páez, H. M. Poggi-Varaldo, Improvement of biohydrogen production from solid wastes by intermittent venting and gas flushing of batch reactors headspace. Environ. Sci. Technol. 2006; 40: 3409-3415
[5] H. M. Poggi-Varaldo, A. Carmona-Martínez, A. L. Vázquez-Larios, O. Solorza-Feria, Effect of inoculum type on the performance of a microbial fuel cell fed with spent organic extracts from hydrogenogenic fermentation of organic solid wastes. J. New Mater. Electrochem. Syst. 2009; 12: 49-54
[6] A. L. Vazquez-Larios, O. Solorza-Feria, G. Vazquez-Huerta, F. J. Esparza-Garcia, E. Rios-Leal, N. Rinderknecht-Seijas, H. M. Poggi-Varaldo, A new design improves performance of a single chamber microbial fuel cell. J. New Mater. Electrochem. Syst. 2010; 13: 219-226
[7] Z. Du, H. Li, T. Gu, A state of the art review on microbial fuel cells: A promising technology for wastewater treatment and bioenergy Biotechnol. Adv. 2007; 25: 464–482
[8] O. Lefebvre, A. Al-Mamun, W. K. Ooi, H. Y. Ng, Z. Tang, D. H.C. Chua, An insight into cathode options for microbial fuel cells. Water Sci Technol. 2008; 57: 2031–2037
[9] S. Ouitrakul, M. Sriyudthsak, S. Charojrochkul, T. Kakizono. Impedance analysis of bio-fuel cell electrodes. Biosens. Bioelectron. 2007; 23: 721-727
[10] P. Belleville, P. J. Strong, P. H. Dare, D. J. Gapes. Influence of nitrogen limitation on performance of a microbial fuel cell. Water Sci. Technol. 2011; 63: 1752-1757
[11] B. E. Logan, J. M. Regan, Microbial challenges and harnessing the metabolic activity of bacteria can provide energy for a variety of applications, once technical and cost obstacles are overcome. Environ. Sci. Technol. 2006; 5172–5180
[12] Y. Yang, G. Sun, M. Xu, Microbial fuel cells come of age. J. Chem. Technol. Biotechnol. 2010; 86: 625-632
[13] M. Zhou, M. Chi, J. Luo, H. He, T. Jin, An overview of electrode materials in microbial fuel cells. J. Power Sources 2011; 196: 4427-4435
[14] B. E. Logan, B. Hamelers, R. Rozendal, U. Schröder, J. Keller, S. Freguia, P. Aelterman, W. Verstraete, K. Rabaey, Microbial fuel cells: Methodology and technology. Environ. Sci. Technol. 2006; 40: 5181-5192
[15] H. Rismani-Yazdi, S. M. Carver, A. D. Christy, O. H. Tuovinen, Cathodic limitations in microbial fuel cells: an overview. J. Power Sources 2008; 180: 683-694
[16] D. Halliday, R. Resnick, J. Walker, *Fundamentals of Physics.* 7th ed. John Wiley & Sons, Inc. New York, ISBN:978-0-471-21643-8, 2005
[17] D. Halliday, R. Resnick, J. Walker, *Fundamentals of Physics.* 9th ed. John Wiley & Sons, Inc. New York, ISBN:978-0-471-21643-8, 2011
[18] D. Jiang, B. Li, Novel electrode materials to enhance the bacterial adhesion and increase the power generation in microbial fuel cells (*MFC*s). Wat. Sci. Technol. 2009; 59.3: 557-563
[19] B. E. Logan, Simultaneous wastewater treatment and biological electricity generation. Water Sci. Technol. 2005; 52: 31-37

[20] H. M. Poggi-Varaldo, A. Vazquez-Larios, O. Solorza-Feria, Microbial fuel cells. In Rodríguez-Varela F.J., Solorza-Feria O., Hernández-Pacheco, E. (Eds). *Fuel cells.* Book Livres, Montréal, Canada, 2010, pp 124-161
[21] F. Li, Y. Sharma, Y. Lei, B. Li, Q. Zhou, Microbial fuel cells: The effects of configurations, electrolyte solutions, and electrode materials on power generation. Appl. Biochem. Biotechnol. 2011; 160: 168–181
[22] C. I. Torres, A. K. Marcus, H. S. Lee, P. Parameswaran, R. Krajmalnik-Brown, B. E. Rittmann, A kinetic perspective on extracellular electron transfer by anode-respiring bacteria. Bioresour. Technol. 2010; 102: 9335–9344
[23] K. Rabaey, G. Lissens, D. S. Steven, W. Verstraete, A microbial fuel cell capable of converting glucose to electricity at high rate and efficiency. Biotechnol. Lett. 2003; 25: 1531–1535
[24] H. Liu, B. E. Logan, Electricity generation using an air-cathode single chamber microbial fuel cell in the presence and absence of a proton exchange membrane. Environ. Sci. Technol. 2004; 38: 4040–4046
[25] B. Min, S. Cheng, B. E. Logan, Electricity generation using membrane and salt bridge microbial fuel cells. Water Res. 2005; 39: 1675–1686
[26] H. Liu, S. Cheng, B. E. Logan, Power generation in fed-batch microbial fuel cells as a function of ionic strength, temperature, and reactor configuration. Environ. Sci. Technol. 2005; 39: 5488–5493
[27] S. Cheng, H. Liu, B. E. Logan, Increased power generation in a continuous flow *MFC* with advective flow through the porous anode and reduced electrode spacing. Environ. Sci. Technol. 2006; 40: 2426–2432
[28] B. E. Logan. *Microbial fuel cells.* John Wiley-Interscience. New Jersey, USA, 2007
[29] D. Jiang, B. Li, Granular activated carbon single-chamber microbial fuel cells (GAC-SC*MFC*s): A design suitable for large-scale wastewater treatment processes. Biochem. Eng. J. 2009; 47: 31-37
[30] J. Wei, L. P., H. Xia, Recent progress in electrodes for microbial fuel cells. Bioresour. Technol. 2011; 102: 9335-9344
[31] S. Hays, F. Zhang, B. E. Logan, Performance of two different types of anodes in membrane electrode assembly microbial fuel cells for power generation from domestic wastewater. J. Power Sources 2011; 195: 8293-8300
[32] Y. Feng, Q. Yang, X. Wang, B. E. Logan, Treatment of carbon fiber brush anodes for improving power generation in air–cathode microbial fuel cells. J. Power Sources 2010; 195: 1841-1844
[33] A. Larrosa-Guerrero, K. Scott, K. P. Katuri, C. Godinez, I. M. Head, T. Curtis, Open circuit versus closed circuit enrichment of anodic biofilms in *MFC*: effect on performance and anodic communities**.** Appl. Microbiol. Biotechnol. 2010; 87: 1699-1713
[34] Y. Liu, F. Harnisch, K. Fricke, U. Schröder, V. Climent, J.M. Feliu, The study of electrochemically active microbial biofilms on different carbon- based anode materials in microbial fuel cells. Biosens. Bioelectron. 2010; 25: 2167-2171
[35] T. Jin, L. Zhou, J. Luo, J, Yang, Y. Zhao, M. Zhou, Hydrazine hydrate chemical reduction as an effective anode modification method to improve the performance of microbial fuel cells. J. Chem. Technol. Biotechnol. 2013; 88: 2075-2081
[36] L. Hsu, B. Chadwick, J. Kagan, R. Thacher, A. Wotawa-Bergen, K. Richter, Scale up considerations for sediment microbial fuel Cells. RSC Adv. 2013; 3: 15947–15954
[37] A. Dewan, H. Beyenal, Z. Lewandowski, Scaling up Microbial Fuel Cells. Environ. Sci. Technol. 2008; 42: 7643–7648
[38] M. Di Lorenzo, K. Scott, T. P. Curtis, I. M. Head, Effect of increasing anode surface area on the performance of a single chamber microbial fuel cell. Chem. Eng. J. 2010; 156: 40–48
[39] K. Rabaey, W. Verstraete, Microbial fuel cells: novel biotechnology for energy generation. Trends Biotechnol. 2005; 23: 291–298
[40] A. L. Vazquez-Larios, O. Solorza-Feria, J. Barrera Cortes, E. Ríos-Leal, M. T. Ponce-Noyola, F. Esparza-García, R. G. González-Huerta, N. Rinderknecht-Seijas, H. M. Poggi-Varaldo, Battelle 9th International Conference on Remediation of Chlorinated and Recalcitrant Compounds, May 19-22, 2014. Monterey, CA, USA. Platform Session H8 "Managing recalcitrant compounds in landfill leachate"
[41] G.W. Castellan, *Physical Chemistry*. 2nd Edition. Addison-Wesley, 1971
[42] I. Bronshtein, K. Semendaiev, *Manual de matemáticas para ingenieros y estudiantes (Handbook of mathematics for engineers and students).* Ediciones de Cultura Popular S.A., Mexico DF, Mexico, 1977
[43] R. Perry, Chemical Engineers Handbook, pp 5.50 & ff 4th ed., McGraw-Hill Co, New York, 1963
[44] G. Hernández-Flores, Interim Report. Sc D Thesis, CINVESTAV-IPN, México, D.F., 2013
[45] H.M. Poggi-Varaldo, L. Valdés, F.J. Esparza-García, G. Fernández-Villagómez, Solid susbtrate anaerobic co-digestion of paper mill sludge, bio-solids, and municipal solid waste. Water Sci. Technol. 1997; 35: 197-204
[46] H.M. Poggi-Varaldo, N. Rinderknecht-Seijas, A differential availability enhancement factor for the evaluation of pollutant availability in soil treatments. Acta Biotechnologica 2003; 23: 271-280
[47] H.M. Poggi-Varaldo, L.M. Alzate-Gaviria, A. Perez-Hernandez, V.G. Nevarez-Morillon, N. Rinderknecht-Seijas, A side-by-side comparison of two systems of sequencing coupled reactors for anaerobic digestion of the organic fraction of municipal solid waste. Waste Manage. Res. 2005; 23: 270-280
[48] APHA. *Standard methods for examination of water and wastewater*. 17th ed. APHA-AWWA-WEF, Washington DC, 1989
[49] D. Montgomery. *Design and analysis of experiments*. 3rd ed John Wiley & Sons, New York, 1991